

Combined LHC/ILC analysis of a SUSY scenario with heavy sfermions

K. Desch^a, J. Kalinowski^b, G. Moortgat-Pick^c, K. Rolbiecki^b, W.J. Stirling^d

^a*Physikalisches Institut, Universität Bonn, D-53115 Bonn, Germany*

^b*Instytut Fizyki Teoretycznej, Uniwersytet Warszawski, PL-00681 Warsaw, Poland*

^c*TH Division, Physics Department, CERN, CH-1211 Geneva 23, Switzerland*

^d*IPPP, University of Durham, Durham DH1 3LE, UK*

July 3, 2018

Abstract

We discuss the potential of analyses at the Large Hadron Collider and the planned International Linear Collider to explore low-energy supersymmetry in a difficult region of the parameter space characterized by masses of the scalar SUSY particles around 2 TeV. Precision analyses of cross sections for light chargino production and forward-backward asymmetries of decay leptons and hadrons at the first stage of the ILC with $\sqrt{s} = 500$ GeV, together with mass information on $\tilde{\chi}_2^0$ and squarks from the LHC, allow us to determine the underlying fundamental gaugino/higgsino MSSM parameters and to constrain the masses of the heavy, kinematically inaccessible sparticles. No assumptions on a specific SUSY-breaking mechanism are imposed. For this analysis the complete spin correlations between production and decay processes must be taken into account.

1 Introduction

Supersymmetry (SUSY) is one of the best-motivated candidates for physics beyond the Standard Model (SM). Low-energy SUSY is well-motivated since it stabilizes the electroweak scale, provides quantitatively accurate unification of gauge couplings as well as a promising cold-dark-matter candidate. Moreover, electroweak precision data [1] and cosmology bounds [2] seem to indicate [3] that at least some of the electroweakly interacting SUSY particles should be rather light and accessible at future colliders. However, since the mechanism of SUSY breaking

is unknown, supersymmetric extensions of the Standard Model contain a large number of unknown parameters, e.g. 105 in the Minimal Supersymmetric Standard Model (MSSM). Specific assumptions on the SUSY-breaking mechanism, in particular about the unification of parameters at the grand-unification (GUT) scale, considerably reduce the number of free parameters, e.g. in the constrained MSSM, often referred to as mSUGRA, where we end up with only four new parameters (and one sign) specified at the unification scale. Experiments at future accelerators, the Large Hadron Collider (LHC) and the International Linear Collider (ILC), will have, however, not only to discover SUSY but also to determine precisely the underlying SUSY-breaking scenario with as few theoretical prejudices as possible.

Particularly challenging are scenarios where the scalar SUSY particle sector is very heavy as required, for instance, in focus-point scenarios (FP) [4] where the gaugino masses are kept relatively small while squarks and sleptons might be too heavy for a direct observation at the ILC. It is therefore particularly interesting to verify whether the interplay of a combined LHC/ILC analysis [5] could shed light on models with heavy sfermions.

Many methods have been worked out to derive the SUSY parameters at collider experiments [6–10]. In [11–16] the chargino and neutralino sectors have been exploited at the ILC to determine the MSSM parameters. However, in most cases only the production processes have been studied and, furthermore, it has been assumed that the masses of the virtual scalar particles are already known. In the case of heavy scalars such assumptions cannot be applied and further observables have to be used to determine the underlying parameters. Studies have been made to exploit the whole production-and-decay process, and angular and energy distributions of the decay products in chargino as well as neutralino channels have been studied in [17–20]. Since such observables depend strongly on the polarization of the decaying particle, the spin correlations between production and decay can have a large influence and have to be taken into account. Exploiting such spin effects, it has been shown in [21] that, once the chargino parameters are known, useful indirect bounds for the mass of the heavy virtual particles could be derived from forward–backward asymmetries of the final lepton $A_{\text{FB}}(\ell)$.

In this paper we discuss a FP-inspired scenario characterized by a ~ 2 TeV scalar particles sector. In addition, the neutralino sector turns out to have very low production cross sections in e^+e^- collisions, so that it might not be fully exploitable. Only the chargino pair production process has high rates at the ILC and all information obtainable from this sector has to be used. In order to assess the possibility of unraveling such a challenging new physics scenario, our analysis is performed entirely at the EW scale, without any reference to the underlying SUSY-breaking mechanism. We measure at the LHC and at the ILC with $\sqrt{s} = 500$ GeV the masses, cross sections and spin-dependent forward–backward asymmetries and analyze the potential of a multiparameter fit to determine the underlying parameters.

The paper is organized as follows. In the next section we first present the studied process, chargino production with leptonic and hadronic decays. We briefly introduce the spin formalism, which is needed for the evaluation of spin-dependent observables. In section 3 the FP-inspired scenario is defined and the expected experimental results at the LHC and the ILC are discussed. In section 4 we perform our numerical analysis and determine the SUSY parameters based on the experimental input. An attempt at testing the $SU(2)$ symmetry relation for the selectron and sneutrino masses using the available information on the squark masses from the LHC and the forward–backward asymmetry measured at the ILC in hadronic decay modes is also discussed. Section 5 summarizes the results.

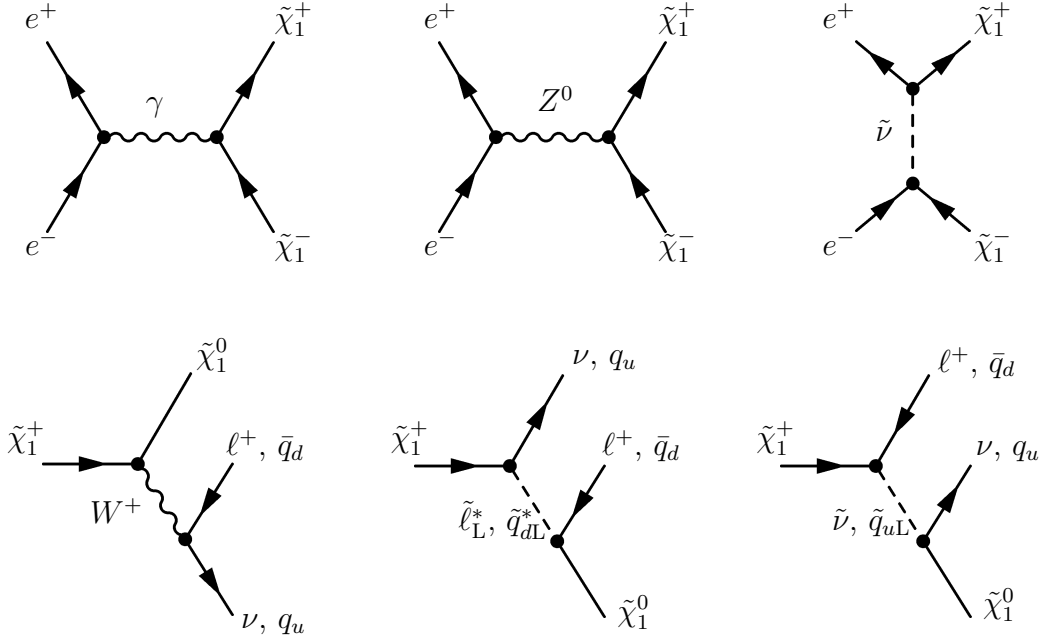


Figure 1: Feynman diagrams for production and for leptonic and hadronic decays of charginos.

2 Strategy overview

2.1 Chargino and neutralino sector

We study chargino production

$$e^- + e^+ \rightarrow \tilde{\chi}_1^+ + \tilde{\chi}_1^-, \quad (1)$$

with subsequent leptonic and hadronic decays

$$\tilde{\chi}_1^+ \rightarrow \tilde{\chi}_1^0 + \ell^+ + \nu \quad \text{and} \quad \tilde{\chi}_1^0 + \bar{q}_d + q_u, \quad (2)$$

$$\tilde{\chi}_1^- \rightarrow \tilde{\chi}_1^0 + \ell^- + \bar{\nu} \quad \text{and} \quad \tilde{\chi}_1^0 + q_d + \bar{q}_u, \quad (3)$$

where $\ell = e, \mu$, $q_u = u, c$, $q_d = d, s$. The corresponding Feynman diagrams are shown in Fig. 1. The production process contains contributions from γ - and Z^0 -exchange in the s -channel and from $\tilde{\nu}$ -exchange in the t -channel. The decay processes are mediated by W^\pm , $\tilde{\ell}_L$, $\tilde{\nu}$ or by \tilde{q}_{dL} , \tilde{q}_{uL} exchange; contributions from Higgs boson exchanges to the production and decay are negligibly small for the first and second generation fermions. For notations, couplings and conventions see, for instance [22].

The neutralino mass eigenstates are defined as $\tilde{\chi}_i^0 = N_{ij}\tilde{\lambda}_j$, where N_{ij} are the elements of the unitary 4×4 matrix which diagonalizes the neutral gaugino–higgsino mass matrix in the

basis $\tilde{\lambda} = (\tilde{B}^0, \tilde{W}^0, \tilde{H}_1^0, \tilde{H}_2^0)$:

$$M_N = \begin{pmatrix} M_1 & 0 & -m_Z \cos \beta \sin \theta_W & m_Z \sin \beta \sin \theta_W \\ 0 & M_2 & m_Z \cos \beta \cos \theta_W & -m_Z \sin \beta \cos \theta_W \\ -m_Z \cos \beta \sin \theta_W & m_Z \cos \beta \cos \theta_W & 0 & -\mu \\ m_Z \sin \beta \sin \theta_W & -m_Z \sin \beta \cos \theta_W & -\mu & 0 \end{pmatrix}, \quad (4)$$

where m_Z denotes the mass of the Z^0 boson, M_1, M_2 are the $U(1), SU(2)$ gaugino mass parameters, μ is the Higgs mass parameter and $\tan \beta = v_2/v_1$, where $v_{1,2}$ are the vacuum expectation values of the two neutral Higgs fields. The chargino mass eigenstates $\tilde{\chi}_i^+ = \begin{pmatrix} \chi_i^+ \\ \tilde{\chi}_i^- \end{pmatrix}$ are defined by $\chi_i^+ = V_{i1}w^+ + V_{i2}h^+$ and $\chi_j^- = U_{j1}w^- + U_{j2}h^-$. Here w^\pm and h^\pm are the two-component spinor fields of the wino and the charged higgsinos, respectively. Furthermore, U_{ij} and V_{ij} are the elements of the unitary 2×2 matrices, which diagonalize the chargino mass matrix:

$$M_C = \begin{pmatrix} M_2 & m_W \sqrt{2} \sin \beta \\ m_W \sqrt{2} \cos \beta & \mu \end{pmatrix}, \quad (5)$$

where m_W denotes the mass of the W^\pm bosons.

2.2 Spin formalism

We study the production process including the subsequent leptonic and hadronic decays. Since in our scenario charginos are very narrow ($\Gamma_{\tilde{\chi}_1^\pm} = 2.3$ keV), the narrow-width approximation is appropriate and contributions from off-shell channels are negligible; this approximation can be tested with several Monte Carlo event generators that include off-shell effects as well as spin correlations [23]. The process can therefore be split into the chargino production and the decay processes. In order to exploit spin-dependent observables, e.g. forward-backward asymmetries of the final leptons and quarks, however, the full spin information of the decaying charginos has to be taken into account. In the following we briefly summarize the required spin formalism. More details as well as the explicit analytic expressions for the chargino production spin density matrix and the decay processes can be found in [17, 18].

The amplitude for the whole process is

$$T = \Delta(\tilde{\chi}_i^+) \Delta(\tilde{\chi}_j^-) \sum_{\lambda_i, \lambda_j} T_P^{\lambda_i \lambda_j} T_{D, \lambda_i} T_{D, \lambda_j}, \quad (6)$$

with the helicity amplitude for the production process $T_P^{\lambda_i \lambda_j}$ and those for the decay processes $T_{D, \lambda_i}, T_{D, \lambda_j}$, and the propagators $\Delta(\tilde{\chi}_i^\pm) = 1/[s_i - m_i^2 + im_i \Gamma_i]$. Here $\lambda_i, s_i, m_i, \Gamma_i$ denote the helicity, four-momentum squared, mass and width of $\tilde{\chi}_i^\pm$. The amplitude squared

$$|T|^2 = |\Delta(\tilde{\chi}_i^+)|^2 |\Delta(\tilde{\chi}_j^-)|^2 \rho^{P, \lambda_i \lambda_j \lambda_i' \lambda_j'} \rho_{\lambda_i' \lambda_i}^D \rho_{\lambda_j \lambda_j'}^D \quad (\text{sum convention used}) \quad (7)$$

is thus composed of the (unnormalized) spin density production matrix

$$\rho^{P, \lambda_i \lambda_j \lambda_i' \lambda_j'} = T_P^{\lambda_i \lambda_j} T_P^{\lambda_i' \lambda_j'*} \quad (8)$$

of $\tilde{\chi}_{i,j}^\pm$, and the decay matrices

$$\rho_{\lambda'_i \lambda_i}^D = T_{D,\lambda_i} T_{D,\lambda'_i}^* \quad \text{and} \quad \rho_{\lambda'_j \lambda_j}^D = T_{D,\lambda_j} T_{D,\lambda'_j}^*. \quad (9)$$

Interference terms between various helicity amplitudes preclude factorization in a production factor $\sum_{\lambda_i \lambda_j} |T_P^{\lambda_i \lambda_j}|^2$ times a decay factor $\sum_{\lambda'_i \lambda'_j} |T_{D,\lambda'_i \lambda'_j}|^2$.

The spin density production matrix $\rho^{P,\lambda_i \lambda_j \lambda'_i \lambda'_j}$ can be decomposed into four parts (for details see [17]):

$$\rho^{P,\lambda_i \lambda_j \lambda'_i \lambda'_j} = P^{\lambda_i \lambda_j \lambda'_i \lambda'_j} + \Sigma_a^{P,\lambda_i \lambda_j \lambda'_i \lambda'_j} + \Sigma_b^{P,\lambda_i \lambda_j \lambda'_i \lambda'_j} + \Sigma_{ab}^{P,\lambda_i \lambda_j \lambda'_i \lambda'_j}, \quad (10)$$

where P denotes a contribution which is independent of chargino polarizations, Σ_a (Σ_b) depends on the polarization of one of the charginos, and Σ_{ab} on both; $a, b = 1, 2, 3$ denote the components (transverse and longitudinal) of the spin vectors. Likewise, the decay matrices $\rho_{\lambda'_i \lambda_i}^D$ and $\rho_{\lambda'_j \lambda_j}^D$ can each be separated into two parts as

$$\rho_{\lambda'_i \lambda_i}^D = D_{\lambda'_i \lambda_i} + \Sigma_{a,\lambda'_i \lambda_i}^D. \quad (11)$$

The amplitude squared $|T|^2$ of the combined processes of production and decays can schematically be written as (with helicity indices suppressed):

$$|T|^2 \sim P D_i D_j + \Sigma_a^P \Sigma_a^D D_j + \Sigma_b^P \Sigma_b^D D_i + \Sigma_{ab}^P \Sigma_a^D \Sigma_b^D, \quad (12)$$

The first product in Eq. (12) is independent of spin correlations between production and decay. The second and third terms describe the correlations between the production and the decay process either of $\tilde{\chi}_i^+$ or $\tilde{\chi}_j^-$ decay and, in the last term correlations between both decay processes are included.

- In the first term of Eq. (12) only scalar products appear, which can be expressed by the Mandelstam variables s, t, u for the production and decay processes. This is the only term that survives in the total cross section, i.e. when all the angles are integrated over.
- In the second (third) term of Eq. (12) the spin vectors relate quantities from the production with those from the decay process. These scalar products cannot be expressed by Mandelstam variables. They contain the angle between the incoming electron and the outgoing lepton or quark in the laboratory system. These terms contribute to spin-dependent observables as, for example, to the forward–backward asymmetry of the final leptons and quarks.
- The last term of Eq. (12) involves the spin vectors of both charginos and leads to spin correlations between the two decay chains of $\tilde{\chi}_i^+$ and $\tilde{\chi}_j^-$.

If the decay of only one chargino, e.g. $\tilde{\chi}_i^+$, is considered, one has to sum over the spin of $\tilde{\chi}_j^-$ so that in Eq. (12) $D_j = 1$ and $\Sigma_b^D = 0$.

2.3 Strategy for the determination of the SUSY parameters

Our aim is to demonstrate the power of forward–backward asymmetries in determining the masses of kinematically inaccessible heavy sleptons. Note, however, that the leptonic forward–backward asymmetry involves the masses of both sneutrinos and selectrons. Therefore the analysis is performed in steps. First we exploit the chargino and neutralino masses and the chargino production cross sections times decay branching fractions, to constrain fundamental parameters of the chargino and neutralino sectors and the sneutrino mass. We then show how the obtained limits on the sneutrino mass and other parameters can be improved by employing the forward–backward asymmetries, measured in leptonic chargino decays at the ILC. This, however, requires the assumption on the $SU(2)$ mass relation for slepton masses. In the last step we make an attempt at testing the $SU(2)$ symmetry relation for the selectron and sneutrino, using the available information on the squark masses from the LHC, and include in addition the forward–backward asymmetry measured at the ILC in hadronic decay modes.

3 Case study with heavy sfermions

3.1 Parameters of the chosen scenario

The following mSUGRA parameters, taken at the GUT scale except for $\tan\beta$, define the MSSM scenario:

$$m_{1/2} = 144 \text{ GeV}, \quad m_0 = 2 \text{ TeV}, \quad A_0 = 0 \text{ GeV}, \quad \tan\beta = 20, \quad \text{sgn}(\mu) = +1. \quad (13)$$

However, our analysis is performed *entirely* within the general MSSM framework, without any reference to the underlying SUSY-breaking mechanism. The parameters at the EW scale are obtained with the help of the SPheno code [25] for $m_t = 178 \text{ GeV}$; furthermore it has been checked with the code micrOMEGA [26] that the lightest neutralino provides a relic cold-dark-matter density consistent with cosmological data. The low-scale gaugino/higgsino/gluino masses as well as the derived masses of SUSY particles are listed in Tables 1 and 2. The charginos and neutralinos as well as the gluino are rather light, whereas the scalar SUSY particles have masses about 2 TeV.

M_1	M_2	M_3	μ	$\tan\beta$	$m_{\tilde{\chi}_1^\pm}$	$m_{\tilde{\chi}_2^\pm}$	$m_{\tilde{\chi}_1^0}$	$m_{\tilde{\chi}_2^0}$	$m_{\tilde{\chi}_3^0}$	$m_{\tilde{\chi}_4^0}$	$m_{\tilde{g}}$
60	121	322	540	20	117	552	59	117	545	550	416

Table 1: *Low-scale gaugino/higgsino/ $\tan\beta$ MSSM parameters, and the resulting chargino, neutralino and gluino masses (all masses are given in GeV).*

3.2 Expectations at the LHC

As can be seen from Tables 1 and 2, all squarks are kinematically accessible at the LHC. The largest squark production cross section is for $\tilde{t}_{1,2}$. However, with stops decaying mainly to $\tilde{g}t$ (with $BR(\tilde{t}_{1,2} \rightarrow \tilde{g}t) \sim 66\%$), where background from top production will be large, no new

m_h	$m_{H,A}$	m_{H^\pm}	$m_{\tilde{\nu}_e}$	$m_{\tilde{e}_R}$	$m_{\tilde{e}_L}$	$m_{\tilde{\tau}_1}$	$m_{\tilde{\tau}_2}$	$m_{\tilde{q}_R}$	$m_{\tilde{q}_L}$	$m_{\tilde{t}_1}$	$m_{\tilde{t}_2}$
119	1934	1935	1994	1996	1998	1930	1963	2002	2008	1093	1584

Table 2: *Masses of the SUSY Higgs particles and scalar SUSY particles (all masses are given in GeV).*

interesting channels are open in their decays. The other squarks decay mainly via $\tilde{g}q$, but since the squarks are very heavy, $m_{\tilde{q}_{L,R}} \sim 2$ TeV, precise mass reconstruction will be difficult. Therefore we conservatively assume that the squark masses can be measured with an error of 50 GeV. Our results do not depend sensitively on this assumption since the mere indication that the scalar quarks are very heavy will be sufficient for narrowing the experimental uncertainty on the slepton sector from the ILC measurements.

In this scenario, the inclusive discovery of SUSY at the LHC is possible mainly because of the large gluino production cross section. Therefore several gluino decay channels can be exploited. The largest branching ratio for the gluino decay in our scenario is a three-body decay into neutralinos, $BR(\tilde{g} \rightarrow \tilde{\chi}_2^0 b\bar{b}) \sim 14\%$, with a subsequent three-body leptonic neutralino decay $BR(\tilde{\chi}_2^0 \rightarrow \tilde{\chi}_1^0 \ell^+ \ell^-)$, $\ell = e, \mu$ of about 6%, see Table 3. In this channel the dilepton edge will be clearly visible, since this process has low backgrounds [5]. The mass difference between the two light neutralinos can be measured from the dilepton edge with an uncertainty of about [24]:

$$\delta(m_{\tilde{\chi}_2^0} - m_{\tilde{\chi}_1^0}) \sim 0.5 \text{ GeV}. \quad (14)$$

Mode	$\tilde{g} \rightarrow \tilde{\chi}_2^0 b\bar{b}$	$\tilde{g} \rightarrow \tilde{\chi}_1^- q_u \bar{q}_d$	$\tilde{\chi}_1^+ \rightarrow \tilde{\chi}_1^0 \bar{q}_d q_u$	$\tilde{\chi}_2^0 \rightarrow \tilde{\chi}_1^0 \ell^+ \ell^-$	$\tilde{t}_{1,2} \rightarrow \tilde{g}t$	$\tilde{\chi}_1^- \rightarrow \tilde{\chi}_1^0 \ell^- \bar{\nu}_\ell$
BR	14.4%	10.8%	33.5%	3.0%	66%	11.0%

Table 3: *Branching ratios for some important decay modes in the studied MSSM scenario, $\ell = e, \mu, \tau$, $q_u = u, c$, $q_d = d, s$. Numbers are given for each family separately.*

Other frequent gluino decays are into the light chargino and jets, with $BR(\tilde{g} \rightarrow \tilde{\chi}_1^\pm qq') \sim 20\%$ for qq' in the first two families, and about 3% in the third, with a subsequent leptonic chargino decay $BR(\tilde{\chi}_1^\pm \rightarrow \tilde{\chi}_1^0 \ell^\pm \nu_\ell)$, $\ell = e, \mu$ of about 11%. However, exploiting this channel for the chargino-neutralino mass difference measurement is very difficult. First, because of the escaping neutrino, and second, because of a genuine 3-body chargino decay in our scenario. To our knowledge, the only attempt to determine chargino mass at the LHC required $\tilde{\chi}^\pm \rightarrow \tilde{\chi}_1^0 W^\pm \rightarrow \tilde{\chi}_1^0 \ell^\pm \nu_\ell$ with W^\pm on-shell arriving at a statistical accuracy of ~ 25 GeV [27].

In both gluino decay channels the spin measurements via angular correlations [19, 20] of decay products should provide evidence for the spin 1/2 character of the intermediate particles assuring us that the underlying SUSY scenario is realized.

Finally, the gluino mass can be reconstructed in a manner similar to the one proposed in [29], where the SPS1a scenario is analyzed. Although our scenario is different, the precision in both is limited by systematic uncertainties due to hadronic energy scale and a similar relative uncertainty of $\sim 2\%$ can be expected.

3.3 Expectations at the ILC

At the ILC with $\sqrt{s} \leq 500$ GeV, only light charginos and neutralinos are kinematically accessible. However, in this scenario the light neutralino sector is characterized by very low production cross sections. For example, at 500 GeV and $(P_{e^-}, P_{e^+}) = (-90\%, +60\%)$ beam polarization we obtain $\sigma(\tilde{\chi}_1^0 \tilde{\chi}_2^0) = 0.93$ fb, $\sigma(\tilde{\chi}_2^0 \tilde{\chi}_2^0) = 0.49$ fb; for other beam polarization and/or lower collider energy the cross sections are even lower. This is due to the almost pure gaugino nature of light neutralinos ($\tilde{\chi}_1^0 \sim 99\% \tilde{B}^0$, $\tilde{\chi}_2^0 \sim 97\% \tilde{W}^0$) with suppressed couplings to the s -channel Z -boson, while the t - and u -channel selectron exchange is small because of the heavy selectron mass. Only the $\tilde{\chi}_3^0 \tilde{\chi}_4^0$ channel (because of opposite CP parities of $\tilde{\chi}_3^0$ and $\tilde{\chi}_4^0$) could have an appreciable cross section above its threshold $\sqrt{s} \sim 1100$ GeV.

Only the chargino pair production process has high rates at the ILC and all information obtainable from this sector has to be used. We constrain our analysis to the first stage of the ILC with $\sqrt{s} \leq 500$ GeV and study only the $\tilde{\chi}_1^+ \tilde{\chi}_1^-$ production

$$e^+ e^- \rightarrow \tilde{\chi}_1^+ \tilde{\chi}_1^-, \quad (15)$$

with subsequent chargino decays

$$\tilde{\chi}_1^- \rightarrow \tilde{\chi}_1^0 e^- \bar{\nu}_e, \tilde{\chi}_1^0 \mu^- \bar{\nu}_\mu, \tilde{\chi}_1^0 d \bar{u} \quad \text{and} \quad \tilde{\chi}_1^0 s \bar{c} \quad (16)$$

and the corresponding charge conjugate $\tilde{\chi}_1^+$ decays, for which the analytical formulae, including the complete spin correlations, are given in a compact form, e.g. in [17].

3.3.1 Mass measurements

The chargino mass can be measured at $\sqrt{s} = 350$ and 500 GeV in the continuum, with an error of about 0.5 GeV [28, 30]. This can serve to optimize the ILC scan at the threshold [31] which, because of the steepness of the s -wave excitation curve in $\tilde{\chi}_1^+ \tilde{\chi}_1^-$ production, can be used to determine the light chargino mass very precisely, to about [30]:

$$m_{\tilde{\chi}_1^\pm} = 117.1 \pm 0.1 \text{ GeV}. \quad (17)$$

The mass of the lightest neutralino $m_{\tilde{\chi}_1^0}$ can be derived via the decays of the light chargino, either from the energy distribution of the lepton ℓ^- ($BR(\tilde{\chi}_1^- \rightarrow \tilde{\chi}_1^0 \ell^- \bar{\nu}_\ell) \sim 11\%$, see Table 3) or from the invariant mass distribution of the two jets in hadronic decays ($BR(\tilde{\chi}_1^- \rightarrow \tilde{\chi}_1^0 q d \bar{q} u) \sim 33\%$, see Table 3). We take [30]

$$m_{\tilde{\chi}_1^0} = 59.2 \pm 0.2 \text{ GeV}. \quad (18)$$

Together with the information from the LHC, Eq. (14), a mass uncertainty for the second lightest neutralino of about

$$m_{\tilde{\chi}_2^0} = 117.1 \pm 0.5 \text{ GeV} \quad (19)$$

can be assumed.

3.3.2 Experimental uncertainties for the cross sections

Table 4 lists the expected chargino production cross sections and forward–backward asymmetries for different beam energies and polarization configurations, derived with the nominal values of parameters. Experimentally we identify the chargino pair production process, $e^+e^- \rightarrow \tilde{\chi}_1^+ \tilde{\chi}_1^-$, in the fully leptonic ($\ell^+ \nu \tilde{\chi}_1^0 \ell^- \bar{\nu} \tilde{\chi}_1^0$) and semileptonic ($\ell \nu \tilde{\chi}_1^0 q \bar{q}' \tilde{\chi}_1^0$) final states (where $\ell = e, \mu$). We estimate an overall selection efficiency of 50%. For both final states, W^+W^- production is expected to be the dominant SM background. The fully leptonic channel is more challenging, owing to the absence of mass constraints. Its efficient selection needs further experimental study. However, the fully leptonic channel is not essential for this analysis, as its relative contribution to the overall rate is only $\sim 14\%$. For the semileptonic (slc) final state, this background can be efficiently reduced from the reconstruction of the hadronic invariant mass. In Table 4, we list cross sections multiplied by the branching fraction $B_{slc} = 2 \times BR(\tilde{\chi}_1^+ \rightarrow \tilde{\chi}_1^0 \bar{q}_d q_u) \times BR(\tilde{\chi}_1^- \rightarrow \tilde{\chi}_1^0 \ell^- \bar{\nu}) + [BR(\tilde{\chi}_1^- \rightarrow \tilde{\chi}_1^0 \ell^- \bar{\nu})]^2 \sim 0.34$ (ℓ, q_d, q_u include the first two families of leptons and quarks) including an $e_{slc} = 50\%$ selection efficiency. The error includes, added in quadrature, the statistical uncertainty based on numbers of identified events for $\mathcal{L} = 200 \text{ fb}^{-1}$ in each polarization configuration, $(P_{e^-}, P_{e^+}) = (-90\%, +60\%)$ and $(+90\%, -60\%)$, and a relative uncertainty in the polarization of $\Delta P_{e^\pm}/P_{e^\pm} = 0.5\%$ [33]. Since the production rates are high, the total uncertainties are rather small; see Table 4.

\sqrt{s}/GeV	(P_{e^-}, P_{e^+})	$\sigma(\tilde{\chi}_1^+ \tilde{\chi}_1^-)/\text{fb}$	$\sigma(\tilde{\chi}_1^+ \tilde{\chi}_1^-) B_{slc} e_{slc}/\text{fb}$	$A_{\text{FB}}(\ell^-)/\%$	$A_{\text{FB}}(\bar{c})/\%$
350	$(-90\%, +60\%)$	6195.5	1062.5 ± 4.0	4.42 ± 0.29	4.18 ± 0.74
	$(+90\%, -60\%)$	85.0	14.6 ± 0.7	–	–
500	$(-90\%, +60\%)$	3041.5	521.6 ± 2.3	4.62 ± 0.41	4.48 ± 1.05
	$(+90\%, -60\%)$	40.3	6.9 ± 0.4	–	–

Table 4: Cross sections for the process $e^+e^- \rightarrow \tilde{\chi}_1^+ \tilde{\chi}_1^-$ and forward–backward asymmetries (A_{FB}) in the leptonic $\tilde{\chi}_1^- \rightarrow \tilde{\chi}_1^0 \ell^- \bar{\nu}$ and hadronic $\tilde{\chi}_1^- \rightarrow \tilde{\chi}_1^0 s \bar{c}$ decay modes, for different beam polarization P_{e^-}, P_{e^+} configurations at centre-of-mass energies $\sqrt{s} = 350 \text{ GeV}$ and 500 GeV at the ILC. Concerning the errors, see text.

3.3.3 Experimental uncertainties for the forward–backward asymmetries

Figure 2 shows the expected forward–backward asymmetries measured in the leptonic and hadronic decay channels as functions of the sneutrino mass; for illustration, the dashed line in the left panel demonstrates that spin correlations between production and decay must be taken into account for a proper interpretation of the experimental data. In the case of leptonic decay the $SU(2)$ relation on slepton masses

$$m_{\tilde{e}_L}^2 = m_{\tilde{\nu}_e}^2 + m_Z^2 \cos(2\beta)(-1 + \sin^2 \theta_W) \quad (20)$$

has been assumed, while for the hadronic decay the squark masses are taken to be fixed by the LHC measurement.

The forward–backward asymmetry is defined as:

$$A_{\text{FB}} = \frac{\sigma_{\text{F}} - \sigma_{\text{B}}}{\sigma_{\text{F}} + \sigma_{\text{B}}}, \quad (21)$$

where σ_{F} and σ_{B} are the acceptance-corrected cross sections. The statistical error on A_{FB} , assuming a binomial distribution, is given by

$$\Delta(A_{\text{FB}})^{\text{stat}} = 2\sqrt{\epsilon(1-\epsilon)/N}, \quad (22)$$

where $\epsilon = \sigma_{\text{F}}/(\sigma_{\text{F}} + \sigma_{\text{B}})$ and N denotes the number of selected events. Errors due to uncertainties of beam polarization and squark masses are negligible.

For the *leptonic* forward–backward asymmetry, σ_{F} and σ_{B} are the acceptance-corrected cross sections for the e^-/μ^- from $\tilde{\chi}_1^-$ being observed in the forward (F) and backward (B) hemisphere, respectively, for $\ell^-\bar{\nu}\tilde{\chi}_1^0q\bar{q}'\tilde{\chi}_1^0$ and $\ell^-\bar{\nu}\tilde{\chi}_1^0\ell^+\nu\tilde{\chi}_1^0$ final states. For the $\ell^+\nu\tilde{\chi}_1^0q\bar{q}'\tilde{\chi}_1^0$ final state, in which ℓ^+ comes from $\tilde{\chi}_1^+$ decay, the condition is that the positive lepton is observed in the backward (F) or forward (B) direction.

The *hadronic* forward–backward asymmetry has been analyzed if one flavour of the hadronic 2-jet system can be identified. Since the expected vertex-detector performance is excellent at the ILC, charm-tagging from secondary vertices and displaced tracks can be envisaged. This allows us to measure the forward–backward asymmetry of the c/\bar{c} -jet in each of the different semileptonic decays $\ell^+\nu\tilde{\chi}_1^0\bar{c}s\tilde{\chi}_1^0$ and $\ell^-\bar{\nu}\tilde{\chi}_1^0c\bar{s}\tilde{\chi}_1^0$. Note that the charge sign of the c -jet can be inferred from the lepton charge of the other chargino decay and does not have to be measured through jet- or vertex-charge techniques. Taking the results from [34], c -jets can be identified with an efficiency of 50% at a purity of 80% in Z -decays at rest. The purity from chargino and W decays is larger, since the ratio of true charm/non-charm jets is $\sim 1/3$ (compared to $\sim 1/5$ for Z decays). In this analysis, we assume an overall selection efficiency for $\ell\nu\tilde{\chi}_1^0cs\tilde{\chi}_1^0$ of 20%, corresponding to a c -tag efficiency of 40% for a selection efficiency of 50%. In Table 4 the asymmetries are listed only for the $(P_{e^-}, P_{e^+}) = (-90\%, +60\%)$ case, since the cross sections for the opposite polarization are very small and the statistical errors become very large. Consequently we do not include them in the following analysis.

4 Parameter determination

In the following we apply multiparameter fits to determine the underlying SUSY parameters.

- In the first step we use only the masses $\tilde{\chi}_1^\pm$, $\tilde{\chi}_1^0$, $\tilde{\chi}_2^0$ and the chargino pair production cross section, including the full leptonic and the semileptonic decays as observables. A four-parameter fit for the parameters M_1 , M_2 , μ and $m_{\tilde{\nu}}$ has been applied.
- In the second step we include as an additional observable the leptonic forward–backward asymmetry. Only the semileptonic and purely leptonic decays were used. The $SU(2)$ relation between the two virtual masses $m_{\tilde{\nu}}$ and $m_{\tilde{e}_L}$ has been applied as an external constraint.
- As an attempt to test the $SU(2)$ mass relation for the slepton and sneutrino masses, in the last step both the leptonic and hadronic forward–backward asymmetries have been used. A six-parameter fit for the parameters M_1 , M_2 , μ , $m_{\tilde{\nu}}$, $m_{\tilde{e}_L}$ and $\tan\beta$ has been applied.

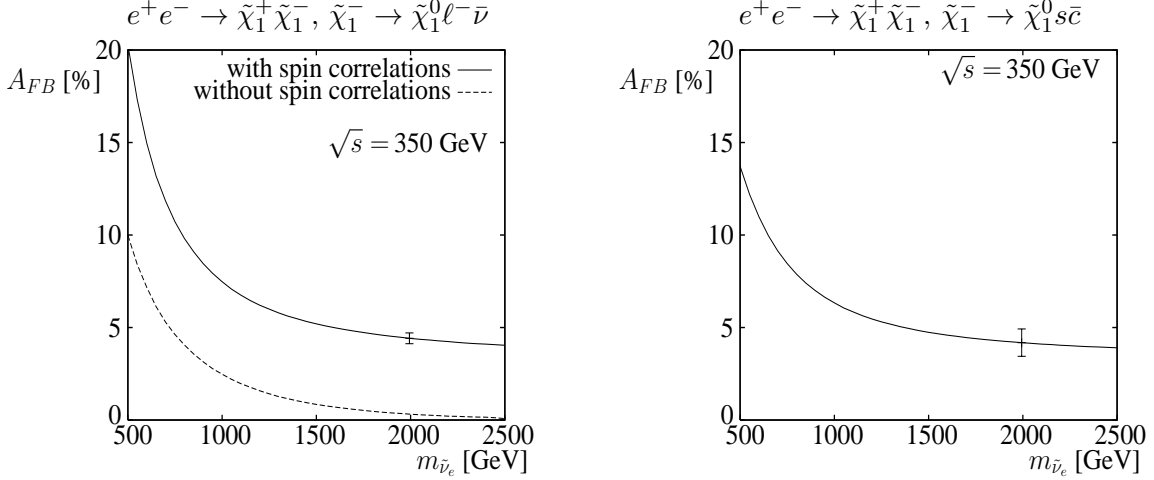


Figure 2: Forward-backward asymmetry of e^- in the process $e^+e^- \rightarrow \tilde{\chi}_1^+ \tilde{\chi}_1^-, \tilde{\chi}_1^- \rightarrow \tilde{\chi}_1^0 \ell^- \bar{\nu}$ (left panel) and of \bar{c} -jet in the process $e^+e^- \rightarrow \tilde{\chi}_1^+ \tilde{\chi}_1^-, \tilde{\chi}_1^- \rightarrow \tilde{\chi}_1^0 s \bar{c}$ (right panel), shown as a function of $m_{\tilde{\nu}_e}$ at $\sqrt{s} = 350$ GeV and polarized beams $(P_{e^-}, P_{e^+}) = (-90\%, +60\%)$. In the left panel the mass of the other scalar virtual particle, $m_{\tilde{e}_L}$, which contributes to the decay process, has been assumed to fulfill the $SU(2)$ mass relation, Eq. (20), while in the right panel the mass of the squark is kept fixed as measured at the LHC. For nominal value of $m_{\tilde{\nu}_e} = 1994$ GeV the expected experimental errors are shown, see Eq. 22. For illustration only, the dashed line in the left panel shows that neglecting spin correlations would lead to a completely wrong interpretation of the experimental data.

4.1 Parameter fit without using the forward-backward asymmetry

We use as observables the masses $m_{\tilde{\chi}_1^\pm}$, $m_{\tilde{\chi}_1^0}$, $m_{\tilde{\chi}_2^0}$ and the polarized chargino cross section multiplied by the branching ratios of semileptonic chargino decays: $\sigma(e^+e^- \rightarrow \tilde{\chi}_1^+ \tilde{\chi}_1^-) \times B_{slc}$, with $B_{slc} = 2 \times BR(\tilde{\chi}_1^+ \rightarrow \tilde{\chi}_1^0 \bar{q}_d q_u) \times BR(\tilde{\chi}_1^- \rightarrow \tilde{\chi}_1^0 \ell^- \bar{\nu}) + [BR(\tilde{\chi}_1^- \rightarrow \tilde{\chi}_1^0 \ell^- \bar{\nu})]^2 \sim 0.34$, $\ell = e, \mu$, $q_u = u, c$, $q_d = d, s$, with selection efficiency 50%, as given in Table 4. Note that the chargino branching ratios are not sensitive functions of sfermion masses mediating their decays, since we know from the LHC that sfermions are very heavy. We take into account the 1σ statistical error based on $\mathcal{L} = 200 \text{ fb}^{-1}$ for each polarization configuration, a relative uncertainty in polarization of $\Delta P_{e^\pm}/P_{e^\pm} = 0.5\%$ [33] and an experimental efficiency of 50%; see Table 4.

We apply a four-parameter fit for the parameters M_1 , M_2 , μ and $m_{\tilde{\nu}_e}$ for fixed values of $\tan\beta = 5, 10, 15, 20, 25, 30, 50$ and 100. Fixing $\tan\beta$ is necessary for a proper convergence of the fitting procedure [32] because of strong correlations among parameters. We perform a χ^2 test

$$\chi^2 = \sum_{\substack{i=\text{LR,RL} \\ j=350,500}} \left(\frac{\sigma(ij) - \sigma(ij)^{\text{th}}}{\Delta\sigma(ij)} \right)^2 + \sum_{i=\tilde{\chi}_1^\pm, \tilde{\chi}_1^0, \tilde{\chi}_2^0} \left(\frac{m_i - m_i^{\text{th}}}{\Delta m_i} \right)^2, \quad (23)$$

where in the first term $i = \text{LR, RL}$ denote (e^-, e^+) polarization configurations $(-90\%, +60\%)$ and $(+90\%, -60\%)$ respectively, and $j = 350, 500$ denote the c.m. energy in GeV; $\sigma(ij)$, m_i and $\Delta\sigma(ij)$, Δm_i are the corresponding cross sections and masses and their uncertainties; see Table 4 and Eqs. (17)–(19).

It turns out that for $\tan\beta < 1.7$ the measurements are inconsistent with theoretical predic-

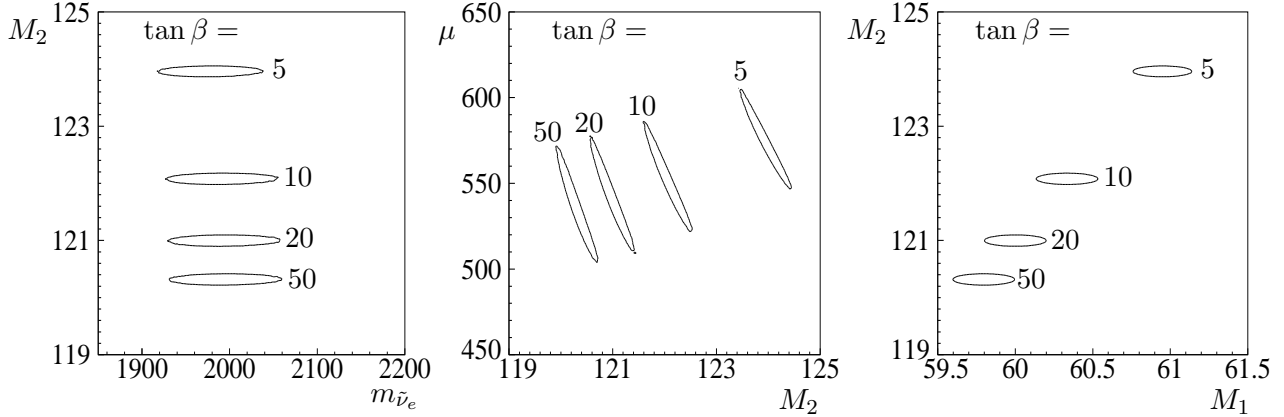


Figure 3: Migration of 1σ contours for $\tan\beta = 5, 10, 20, 50$ with the other two parameters fixed at the values determined by the minimum of χ^2 for each $\tan\beta$.

tions at least at the 1σ level. The corresponding 1σ constraints from cross sections and light neutralino and chargino mass measurements for the underlying parameters are as follows

$$\begin{aligned} 59.4 \leq M_1 \leq 62.2 \text{ GeV}, \quad 118.7 \leq M_2 \leq 127.5 \text{ GeV}, \\ 450 \leq \mu \leq 750 \text{ GeV}, \quad 1800 \leq m_{\tilde{\nu}_e} \leq 2210 \text{ GeV}. \end{aligned} \quad (24)$$

Owing to the strong gaugino component of $\tilde{\chi}_1^\pm$ and $\tilde{\chi}_{1,2}^0$, the parameters M_1 and M_2 are determined reasonably well, with a relative uncertainty of $\sim 3\%$ and $\sim 5\%$. The higgsino parameter μ as well as $m_{\tilde{\nu}_e}$ are determined to a lesser degree of precision, with relative errors of $\sim 30\%$ and 10% . Note, however, that large errors are partly due to migration of the fitted central values of the parameters with $\tan\beta$. Figure 3 shows the migration of 1σ contours¹ in $m_{\tilde{\nu}_e}$ - M_2 (left), M_2 - μ (middle) and M_1 - M_2 (right), the other two parameters being fixed at the values determined by the minimum of χ^2 for $\tan\beta$ changing from 5 to 10, 20 and 50. Beyond $\tan\beta = 50$, the migration is negligible. Varying $\tan\beta$ between 5 and 50 leads to a shift ~ 1 GeV of the fitted central M_1 value and ~ 3.5 GeV of M_2 , effectively increasing their experimental errors, while the migration effect for μ and $m_{\tilde{\nu}_e}$ is much weaker.

4.2 Parameter fit including the leptonic forward-backward asymmetry

We now extend the fit by using as additional observable the leptonic forward-backward asymmetry for polarized beams (-90% , $+60\%$). We include final-state electrons and muons, assuming equal masses of selectrons and smuons, and we include decays of both charginos. The $SU(2)$ relation between selectron and sneutrino masses has been assumed, see Eq. (20). The parameter ranges found in the previous step are scanned and accepted if $\chi_{\text{AFB}}^2 \leq 1$ after inclusion of forward-backward asymmetry according to

$$\chi_{\text{AFB}}^2 = \chi^2 + \sum_i \left(\frac{A_{\text{FB}}(i) - A_{\text{FB}}(i)^{\text{th}}}{\Delta A_{\text{FB}}(i)} \right)^2, \quad (25)$$

¹Note that these plots are 2-dim cuts of a 4-dim hypersurface for each $\tan\beta$ value and they may give a false impression that errors are smaller than that in Eq. (24).

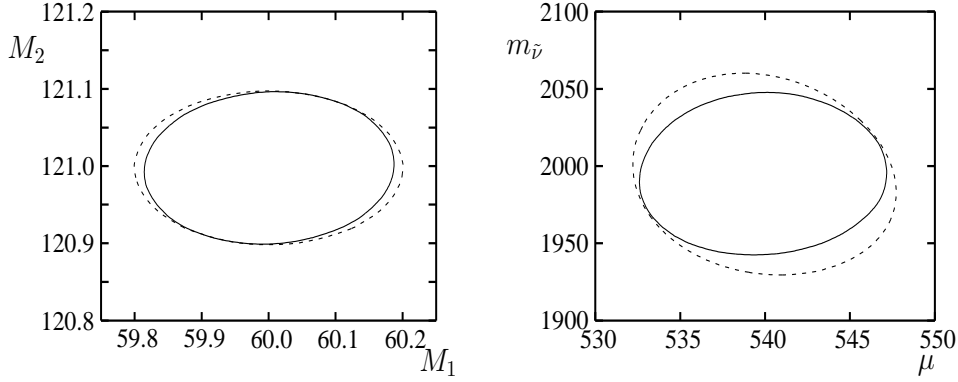


Figure 4: *Two 2-dim cuts in $\{M_1-M_2\}$ and $\{\mu-m_{\tilde{\nu}}\}$ planes of the 1σ hypersurface before (dashes) and after (solid) including the leptonic A_{FB} in the fit for fixed $\tan\beta = 20$ and the other parameters taken at the values determined by the minimum of χ^2 .*

where χ^2 is defined as in Eq. (23), and the sum over i includes A_{FB} measured for both electrons and muons at c.m. energies of 350 and 500 GeV. The terms $A_{\text{FB}}(i)$ and $\Delta A_{\text{FB}}(i)$ are the corresponding experimental forward–backward asymmetries and their uncertainties; see Table 4. For the forward–backward asymmetries the errors due to the uncertainty of beam polarization, although very small with respect to the statistical one, are also included in the χ^2 test. The effect of including the leptonic FB asymmetry in the fit is illustrated in Fig. 4 for two 2-dim cuts of the 1σ hypersurface at *fixed* $\tan\beta = 20$. As expected, the range of $m_{\tilde{\nu}}$ is most affected, although changes of contours are not large. However, the main virtue of including A_{FB} , not visible in this Figure, is *constraining* $\tan\beta$. No assumption on $\tan\beta$ has to be made in the fit since for too small or too large a value of $\tan\beta$ the wrong value of A_{FB} is predicted. As a result, including the forward–backward asymmetries in the multiparameter fit strongly improves the results. We find

$$\begin{aligned}
 59.7 \leq M_1 \leq 60.35 \text{ GeV}, \quad 119.9 \leq M_2 \leq 122.0 \text{ GeV}, \quad 500 \leq \mu \leq 610 \text{ GeV}, \\
 1900 \leq m_{\tilde{\nu}_e} \leq 2100 \text{ GeV}, \quad 14 \leq \tan\beta \leq 31.
 \end{aligned}
 \tag{26}$$

In particular, $\tan\beta$ is constrained from below rather well. The constraints for the mass $m_{\tilde{\nu}_e}$ are improved by a factor of about 2 and for gaugino mass parameters M_1 and M_2 by a factor of about 5, as compared to the results of Section 4.1 with unconstrained $\tan\beta$. The error for the higgsino mass parameter μ also decreases significantly. From Eq. (26) we obtain the following predictions for the heavy charginos/neutralinos

$$506 \leq m_{\tilde{\chi}_3^0} \leq 615 \text{ GeV}, \quad 512 \leq m_{\tilde{\chi}_4^0} \leq 619 \text{ GeV}, \quad 514 \leq m_{\tilde{\chi}_2^\pm} \leq 621 \text{ GeV}.
 \tag{27}$$

These sparticles are only kinematically accessible with non-negligible cross sections at a phase-2 ILC.

4.3 Parameter fit including the hadronic and leptonic forward–backward asymmetries: test of $SU(2)$

4.3.1 Parameter fit including the leptonic A_{FB}

In principle the $SU(2)$ relation can be tested by employing the forward–backward asymmetries measured in hadronic and leptonic decay modes of produced chargino. With the constraints for the squark masses from the LHC, the hadronic forward–backward asymmetry could be used to control the sneutrino mass and the leptonic forward–backward asymmetry to derive constraints on the selectron mass. However, with the foreseen experimental accuracies, testing the $SU(2)$ relation turns out to be very challenging because our measurements do not sufficiently constrain all 6 parameters simultaneously. Therefore, we perform a scan of the parameter space and calculate $\chi_{A_{\text{FB}}}^2$ according to Eq. (25), i.e. taking light chargino and neutralino masses (Eqs. (17-19)), and 4 cross section measurements and 2 leptonic forward–backward asymmetry measurements (entries in columns 3 and 4 of Table 4). From $\chi_{A_{\text{FB}}}^2 = 1$ we derive the following constraints:

$$\begin{aligned} 59.30 \leq M_1 \leq 60.80 \text{ GeV}, \quad 117.8 \leq M_2 \leq 124.2 \text{ GeV}, \quad 420 \leq \mu \leq 950 \text{ GeV}, \\ 1860 \leq m_{\tilde{\nu}_e} \leq 2200 \text{ GeV}, \quad m_{\tilde{e}_L} \geq 1400 \text{ GeV}, \quad \tan \beta \geq 11. \end{aligned} \quad (28)$$

As we can see, without the $SU(2)$ relation the upper limits on the selectron mass and $\tan \beta$ cannot be established since a change of these parameters for high values can be compensated by small changes of other parameters. Limits for the parameter μ are also very poor. The parameters M_1 and M_2 are nevertheless quite well determined, with an accuracy of the order of a few per cent, thanks to tight experimental mass constraints on the light chargino and neutralinos.

4.3.2 Parameter fit including the leptonic and hadronic A_{FB}

Including hadronic forward–backward asymmetry (two entries in the last column of Table 4) improves the constraints as follows:

$$\begin{aligned} 59.45 \leq M_1 \leq 60.80 \text{ GeV}, \quad 118.6 \leq M_2 \leq 124.2 \text{ GeV}, \quad 420 \leq \mu \leq 770 \text{ GeV}, \\ 1900 \leq m_{\tilde{\nu}_e} \leq 2120 \text{ GeV}, \quad m_{\tilde{e}_L} \geq 1500 \text{ GeV}, \quad 11 \leq \tan \beta \leq 60. \end{aligned} \quad (29)$$

The most significant change is for the sneutrino mass, for which error bars become smaller by $\sim 50\%$. Also an upper limit on $\tan \beta$ is found, which has the effect of improving the upper limit on μ significantly and slightly lowering the limits for M_1 and M_2 . However we do not get an upper limit for the selectron mass. Nevertheless, the results for the selectron and sneutrino masses are consistent with the $SU(2)$ relation. The hadronic forward–backward asymmetry would be much more useful with more precise measurements, which is very challenging experimentally.

5 Conclusions

We showed a method for determining the MSSM parameters in scenarios with heavy scalar particles where only a small part of the particle spectrum is kinematically accessible at the

ILC. Such scenarios appear very challenging, since only a very limited amount of experimental information is accessible about the SUSY sector. However, a careful exploitation of data leads to significant constraints for unknown parameters. A very powerful tool in this kind of analysis turns out to be the forward–backward asymmetry. The proper treatment of spin correlations between the production and the decay is necessary in this context. This asymmetry is strongly dependent on the mass of the exchanged heavy particle. If the $SU(2)$ constraint is applied, the slepton masses can be determined to a precision of about 5% for masses around 2 TeV at the ILC running at 500 GeV, i.e. one eighth of the energy necessary for slepton pair production. Also the derived constraints on heavy chargino/neutralinos may provide the physics argument for a second stage of the ILC.

The $SU(2)$ assumption on the left-selectron and sneutrino masses could in principle be tested by combining the leptonic forward–backward asymmetry with the hadronic forward–backward asymmetry for which the squark masses are measured at the LHC. However, with current estimates for the efficiency and purity of charm tagging at the ILC, this test is not very stringent. With significantly better charm-tagging performance more sensitive tests could be performed.

Our analysis stresses the important role of the LHC/ILC interplay, since neither of these colliders alone can provide us with the data needed to determine the SUSY parameters in such scenarios with heavy sfermions without tight model assumptions.

Acknowledgments

We thank G. Polesello for many stimulating discussions. JK and GMP thank the Aspen Center for Physics where part of this work was performed. JK and KR have been supported by the Polish Ministry of Science and Higher Education Grant No 1 P03B 108 30 for the years 2006-2008 and 115/E-343/SPB/DESY/P-03/DWM517/2003-2005.

References

- [1] ALEPH, DELPHI, L3, OPAL and SLD Collaborations and LEPEW, SLDEW and SLD Heavy Flavour Working Groups, *Precision electroweak measurements on the Z resonance*, Phys. Rept. **427** (2006) 257
- [2] C. L. Bennett *et al.*, *Astrophys. J. Suppl.* **148** (2003) 1; D. N. Spergel *et al.* [WMAP Collaboration], *Astrophys. J. Suppl.* **148** (2003) 175; D. N. Spergel *et al.*, arXiv:astro-ph/0603449.
- [3] J. R. Ellis, S. Heinemeyer, K. A. Olive and G. Weiglein, *JHEP* **0605** (2006) 005 [arXiv:hep-ph/0602220].
- [4] J. L. Feng, K. T. Matchev and T. Moroi, *Phys. Rev. D* **61** (2000) 075005 [arXiv:hep-ph/9909334]; J. L. Feng and F. Wilczek, *Phys. Lett. B* **631** (2005) 170 [arXiv:hep-ph/0507032].
- [5] G. Weiglein *et al.* [LHC/LC Study Group], *Phys. Rept.* **426** (2006) 47 [arXiv:hep-ph/0410364].

- [6] T. Tsukamoto, K. Fujii, H. Murayama, M. Yamaguchi and Y. Okada, Phys. Rev. D **51** (1995) 3153.
- [7] J. L. Feng, M. E. Peskin, H. Murayama and X. Tata, Phys. Rev. D **52** (1995) 1418 [arXiv:hep-ph/9502260].
- [8] P. Bechtle, K. Desch and P. Wienemann, Comput. Phys. Commun. **174** (2006) 47 [arXiv:hep-ph/0412012].
- [9] R. Lafaye, T. Plehn and D. Zerwas, arXiv:hep-ph/0404282.
- [10] N. Arkani-Hamed, G. L. Kane, J. Thaler and L. T. Wang, JHEP **0608** (2006) 070 [arXiv:hep-ph/0512190].
- [11] S. Y. Choi, A. Djouadi, H. K. Dreiner, J. Kalinowski and P. M. Zerwas, Eur. Phys. J. C **7** (1999) 123 [arXiv:hep-ph/9806279].
- [12] S. Y. Choi, A. Djouadi, M. Guchait, J. Kalinowski, H. S. Song and P. M. Zerwas, Eur. Phys. J. C **14** (2000) 535 [arXiv:hep-ph/0002033].
- [13] J. L. Kneur and G. Moultaka, Phys. Rev. D **61** (2000) 095003 [arXiv:hep-ph/9907360].
- [14] S. Y. Choi, J. Kalinowski, G. Moortgat-Pick and P. M. Zerwas, Eur. Phys. J. C **22** (2001) 563 [Addendum, *ibid.* C **23** (2002) 769] [arXiv:hep-ph/0108117]; S. Y. Choi, J. Kalinowski, G. Moortgat-Pick and P. M. Zerwas, arXiv:hep-ph/0202039.
- [15] K. Desch, J. Kalinowski, G. Moortgat-Pick, M. M. Nojiri and G. Polesello, JHEP **0402** (2004) 035 [arXiv:hep-ph/0312069].
- [16] H. Baer et al., arXiv:hep-ph/9503479.
- [17] G. Moortgat-Pick, H. Fraas, A. Bartl and W. Majerotto, Eur. Phys. J. C **7** (1999) 113 [arXiv:hep-ph/9804306]; G. Moortgat-Pick, PhD thesis, University of Würzburg, Germany (1999).
- [18] G. Moortgat-Pick and H. Fraas, Phys. Rev. D **59** (1999) 015016 [arXiv:hep-ph/9708481].
- [19] A. J. Barr, Phys. Lett. B **596** (2004) 205 [arXiv:hep-ph/0405052].
- [20] L. T. Wang and I. Yavin, arXiv:hep-ph/0605296.
- [21] G. Moortgat-Pick and H. Fraas, Acta Phys. Polon. B **30** (1999) 1999 [arXiv:hep-ph/9904209]; G. Moortgat-Pick, A. Bartl, H. Fraas and W. Majerotto, Eur. Phys. J. C **18** (2000) 379 [arXiv:hep-ph/0007222].
- [22] H. E. Haber and G. L. Kane, Phys. Rept. **117** (1985) 75.

- [23] W. Kilian, *WHIZARD 1.0: A generic Monte-Carlo integration and event simulation package for multi-particle processes. Manual*, LC-TOOL-2001-039, In *2nd ECFA/DESY Study 1998-2001*, 1924-1980; see also <http://www-ttp.physik.uni-karlsruhe.de/whizard/>; T. Gleisberg, S. Hoche, F. Krauss, A. Schaelicke, S. Schumann and J. C. Winter, *JHEP* **0402** (2004) 056 [arXiv:hep-ph/0311263]; see also <http://www.sherpa-mc.de/>; G. C. Cho, K. Hagiwara, J. Kanzaki, T. Plehn, D. Rainwater and T. Stelzer, *Phys. Rev. D* **73** (2006) 054002 [arXiv:hep-ph/0601063]; see also <http://www.ph.ed.ac.uk/~tplehn/smadgraph/> and <http://web1.pas.rochester.edu/~rain/smagraph/>; for a comparison between the codes and the relevance of off-shell contributions, see K. Hagiwara *et al.*, *Phys. Rev. D* **73** (2006) 055005 [arXiv:hep-ph/0512260].
- [24] K. Kawagoe, M. M. Nojiri and G. Polesello, *Phys. Rev. D* **71** (2005) 035008 [arXiv:hep-ph/0410160].
- [25] W. Porod, *Comput. Phys. Commun.* **153** (2003) 275 [arXiv:hep-ph/0301101].
- [26] G. Belanger, F. Boudjema, A. Pukhov and A. Semenov, arXiv:hep-ph/0405253.
- [27] M. M. Nojiri, G. Polesello and D. R. Tovey, arXiv:hep-ph/0312318.
- [28] H. U. Martyn and G. A. Blair, arXiv:hep-ph/9910416.
- [29] B. K. Gjelsten, D. J. Miller and P. Osland, *JHEP* **0506** (2005) 015 [arXiv:hep-ph/0501033].
- [30] E. Accomando *et al.* [ECFA/DESY LC Physics Working Group Collaboration], *Phys. Rept.* **299** (1998) 1 [arXiv:hep-ph/9705442];
T. Abe *et al.* [American Linear Collider Working Group Collaboration], in *Proc. of the APS/DPF/DPB Summer Study on the Future of Particle Physics*, Snowmass 2001 ed. N. Graf, arXiv:hep-ex/0106056;
J. A. Aguilar-Saavedra *et al.* [ECFA/DESY LC Physics Working Group Collaboration], arXiv:hep-ph/0106315;
K. Abe *et al.* [ACFA Linear Collider Working Group Collaboration], arXiv:hep-ph/0109166.
- [31] W. J. Stirling, *Nucl. Phys. B* **456** (1995) 3.
- [32] F. James and M. Roos, “Minuit’ A System For Function Minimization And Analysis Of The Parameter Errors And Correlations,” *Comput. Phys. Commun.* **10** (1975) 343.
- [33] G. Moortgat-Pick *et al.*, *The role of polarized positrons and electrons in revealing fundamental interactions at the linear collider*, arXiv:hep-ph/0507011, submitted to *Physics Reports*.
- [34] S. Hillert and C. J. S. Damerell, SNOWMASS-2005-ALCPG1403.